Effects of Uniaxial Stress on the Indirect Exciton Spectrum of Silicon†

Lucien D. Laude,* Fred H. Pollak, and Manuel Cardona
Department of Physics, Brown University, Providence, Rhode Island 02912
(Received 1 May 1970)

We have measured the stress dependence of the indirect exciton spectrum of silicon at 77 °K, for static uniaxial compression along the [111], [001], and [110] directions with light polarized parallel and perpendicular to the stress direction, using wavelength modulation. The high stresses reached in this work ($X = 1.8 \times 10^{10}$ dyn cm^{-2}) have enabled us to accurately study the behavior of the $\Gamma_{25'}$ valence-band maxima and the Δ_1 conduction-band minima under stress. The stress splitting of the valence bands is produced by (i) the orbital-strain interaction, which is described by two deformation potentials b_1 and d_1, and (ii) the stress-dependent spin-orbit interaction, described by b_2 and d_2. We find that $b = b_1 + 2b_2 = -(2.10 \pm 0.10)$ eV, $b_2 = -(0.1 \pm 0.15)$ eV, $d = d_1 + 2d_2 = -(4.85 \pm 0.15)$ eV, and $d_2 = -(0.05 \pm 0.25)$ eV. The same measurements yield a value for the shear deformation potential of the Δ_1 conduction-band minimum $\mathcal{E}_2 = -(8.6 \pm 0.4)$ eV. The effect of hydrostatic deformation is interpreted in terms of two deformation potentials: $\mathcal{E}_1 + a_1$ (orbital-strain interaction) and a_2 (stress-dependent spin-orbit interaction). We obtain $\mathcal{E}_1 + a_1 = +(1.5 \pm 0.3)$ eV and $a_2 = 0$. The hydrostatic coefficient of the indirect gap obtained from $\mathcal{E}_1 + a_1$ agrees with hydrostatic pressure measurements. In addition the stress-induced coupling between Δ_1 minima and the neighboring $\Delta_{2'}$ conduction band, described by the deformation potential $|\mathcal{E}_2^*| = (8 \pm 3)$ eV, has been observed. Interpretation of the stress dependence of the intensities on the basis of one ($\Gamma_{15,c}$ or $\Delta_{5,v}$) or two ($\Gamma_{15,c}$ and $\Delta_{5,v}$) intermediate states gives the first conclusive evidence of a contribution of $\Delta_{5,v} \rightarrow \Delta_{1,c}$ virtual transitions to the indirect adsorption edge of this material.

I. INTRODUCTION

The indirect gap of silicon is known to be at 1.16 eV (at 77 °K) and occurs between the $\Gamma_{25'}$ valence-band maxima and a minimum along the Δ_1 conduction band near X_1 [$\vec{k} = 0.86(2\pi/a_0)$ (1, 0, 0,), where a_0 is the lattice constant].[1] The application of a uniaxial stress removes the degeneracy of the $J = \frac{3}{2}$ valence-band state.[2-5] The splitting of this state due to the strain-orbit interaction can be described by two independent deformation potentials b_1 and d_1 appropriate to strains of tetragonal and rhombohedral symmetries, respectively.[6,7] The splitting is also affected by the stress-dependent spin-orbit interaction, whose effect can be described by two additional independent deformation potentials b_2 and d_2.[8] Since the above two interactions have the same form when projected on the space of $J = \frac{3}{2}$ or $J = \frac{1}{2}$, the effect of b_1 and d_1 cannot be separated from that of b_2 and d_2 when one considers only one of the subspaces. Because of the small spin-orbit splitting of this material (0.044 eV at zero stress),[9] the stress-induced coupling between the $J = \frac{3}{2}$ and $J = \frac{1}{2}$ manifolds can be quite large. Hence, the stress-dependent spin-orbit interaction is taken explicitly into account in this experiment in order to determine the deformation potentials. For uniaxial stress along [001] or [110], the degeneracy of the six equivalent Δ_1 conduction-band minima is lifted (interband splitting), an effect which is described by the deformation potential $\mathcal{E}_2$.[10,11] For the case of [111] or [110] stress there is a stress-induced coupling between the Δ_1 and the nearby $\Delta_{2'}$ conduction-band states, resulting in a quadratic shift of the conduction band: This interaction is described by the deformation potential $\mathcal{E}_2^*$.[11,12] In addition to these shear effects, there is also a shift of the indirect edge due to the hydrostatic component of the stress (deformation potentials $\mathcal{E}_1 + a_1$ [10,11] and a_2 [8]). The large stresses used in this work have allowed us to measure accurately the nonlinear effects mentioned above and thus to determine the related deformation potentials. Previous works on silicon[2,4,13] have neglected the stress dependence of the spin-orbit interaction resulting in deformation potentials b and d which correspond, respectively, to $(b_1 + 2b_2)$ and $(d_1 + 2d_2)$. The deformation potentials b and d have been measured by Balslev,[4] whose experiments were confined to about 0.9 $\times 10^{10}$ dyn cm^{-2} at (80 ± 1) °K, Akimchenko and Vdovenkov,[13] and other workers[2]; Balslev, and Akimchenko and Vdovenkov did not specifically analyze nonlinear effects (stress dependence of the spin-orbit splitting and quadratic shift of the $\Delta_{1,c}$ band), which could explain in part the strong disagreement they reported between their measurements of the hydrostatic deformation potential ($\mathcal{E}_1 + a_1 + a_2 = 4.3$ and 4.4 eV) and the value found from hydrostatic pressure measurements.

The intensities of the indirect transitions have also been investigated as a function of stress, assuming two possible indirect mechanisms: one with only one intermediate state (either $\Gamma_{15,c}$ or

$\Delta_{5,v}$), and the other with two intermediate states ($\Gamma_{15,c}$ and $\Delta_{5,v}$). Most of the computed relative intensities of the indirect transitions are found to be consistent with our experimental data for the three stress directions, only if one takes account of the $\Delta_{5,v}$ intermediate state, thus leading to the first conclusive evidence of a significant contribution of $\Delta_{5,v} \rightarrow \Delta_{1,c}$ transitions.

II. EXPERIMENTAL DETAILS

The derivative transmission spectra were observed using a wavelength modulation spectrometer,[14-16] consisting of a 300-line/mm grating monochromator working in second order. The choice of the grating and spectral order was made so as to avoid any structure due to the grating in the wavelength region explored in this work ($\approx 1.0\ \mu$). A water filter was used to eliminate the first-order spectrum. The beam modulation was produced by a vibrating quartz plate mounted directly behind the entrance slit of the monochromator. The detector was a Kodak Ektron PbS photoconductive cell. The detected signals were measured with a Princeton Applied Research HR-8 lock-in amplifier and plotted on a strip-chart recorder. Measurement of the incident beam throughout the considered wavelength range showed no particular structures and a rather smooth and uniform intensity background which did not require any additional signal compensation.

The material (n type) was obtained from Futurecraft Corp.[17] and had a resistivity of 20–50 Ω cm. The samples were x-ray oriented and cut along the [111], [001], and [110] directions to $\pm 1^\circ$ into parallelepipeds of dimensions of $15 \times 1.2 \times 1.0$ mm. Other materials of lower resistivity were also used but the corresponding spectra exhibited much weaker structures. The stresses, applied on samples immersed in liquid nitrogen with a stressing apparatus described elsewhere,[5] ranged up to about 1.8×10^{10} dyn cm^{-2} for the [111] and [110] stresses and 1.1×10^{10} dyn cm^{-2} for the [001] stress for which case external structures, presumably due to the grating, appeared in the spectra at about 1.125 μ and limited our measurements to lower stress. The magnitude of these stresses, together with the use of cooling by immersion, lowered substantially the relative errors and enabled us to obtain accurate values of the deformation potentials mentioned in Sec. I.

III. MEASUREMENTS AND INTERPRETATION

As mentioned in Sec. I, the fundamental edge of silicon is indirect. Therefore, electron-hole coupling states (excitons) are expected to occur between the valence band and the conduction band, giving rise to indirect transitions via an intermediate state either at $\vec{k} = 0$ or $\vec{k} = 0.86\,(2\pi/a_0)\,(1,0,0)$. Selection rules governing these indirect transitions in uniaxially stressed silicon were calculated by Erlbach[18] for all possible phonons. LO-phonon-aided indirect transition can only occur via $\Gamma_{2',c}$; if $\Gamma_{15,c}$ is the intermediate state, then transverse and LA-phonon-aided transitions are allowed. However, both transverse and longitudinal (either acoustic or optic) phonons are allowed for transitions via the Δ_5 valence band. Other intermediate states could be considered, but the probabilities of transitions via these states are very weak because of the large energy denominators. We therefore neglected such processes and limited our investigations to the behavior of the TO-phonon-assisted transitions, which have been reported to be stronger than the TA transitions.[19] Longitudinal-phonon-assisted transitions were not investigated in this work: The energy of the LA-phonon-aided peak should lie 11 meV below the TO-phonon-aided exciton.[20] Recently, Shaklee and Nahory have observed a weak LO exciton line 2 meV below the TO line.[21]

The total Hamiltonian for the $\Gamma_{25'}$ valence band can be written as

$$\mathcal{H} = \mathcal{H}_{SO} + \mathcal{H}_1 + \mathcal{H}_2 \ , \tag{1}$$

where $\mathcal{H}_{SO}$ is the spin-orbit Hamiltonian without stress, $\mathcal{H}_1$ is the orbital-strain Hamiltonian, and $\mathcal{H}_2$ is the stress-dependent spin-orbit Hamiltonian.

It has been shown[2,6] that $\mathcal{H}_1$ can be written as

$$\mathcal{H}_1 = -a_1(\epsilon_{xx}+\epsilon_{yy}+\epsilon_{zz}) - 3b_1[(L_x^2 - \tfrac{1}{3}L^2)\epsilon_{xx} + \text{cp}] - \sqrt{3}d_1[(L_xL_y + L_yL_x)\epsilon_{xy} + \text{cp}] \ , \tag{2}$$

where ϵ_{ij} denotes the components of the strain tensor, $\vec{L}$ is the angular momentum operator, and cp denotes cyclic permutation with respect to the indices x, y, z. The quantity a_1 represents the shift of the orbital bands due to the hydrostatic components of the stress, while b_1 and d_1 are orbital uniaxial deformation potentials.

The expression for $\mathcal{H}_2$ is given by[8]

$$\mathcal{H}_2 = -a_2(\epsilon_{xx}+\epsilon_{yy}+\epsilon_{zz})(\vec{L}\cdot\vec{\sigma}) - 3b_2[(L_x\sigma_x - \tfrac{1}{3}\vec{L}\cdot\vec{\sigma})\epsilon_{xx} + \text{cp}] - \sqrt{3}d_2[(L_x\sigma_y + L_y\sigma_x)\epsilon_{xy} + \text{cp}] \ , \tag{3}$$

where a_2, b_2, and d_2 are additional deformation potentials describing the effects of a strain on the spin-orbit interaction, and $\vec{\sigma}$ is the Pauli matrix vector.

A uniaxial stress may also cause a shift and splitting of the six equivalent Δ_1 conduction-band minima. In the notation of Brooks, the linear term is given by[10]

$$\Delta E = \hat{n}\cdot\{\mathcal{E}_1(\epsilon_{xx}+\epsilon_{yy}+\epsilon_{zz})\vec{1}$$

$$+\mathcal{E}_2[\vec{\epsilon}-\tfrac{1}{3}(\epsilon_{xx}+\epsilon_{yy}+\epsilon_{zz})\vec{1}]\}\cdot\hat{n}\ , \qquad (4)$$

where $\hat{n}$ is the unit vector in the direction of the critical point in $\vec{k}$ space, $\vec{1}$ is the unit diadic, and $\mathcal{E}_1$ and $\mathcal{E}_2$ are hydrostatic and shear-deformation potentials, respectively.[11]

In addition, a nonlinear shift may occur due to the stress-induced coupling between the Δ_1 and $\Delta_{2'}$ conduction bands [the corresponding gap $E(\Delta_{2'})-E(\Delta_1)=0.8$ eV at $\vec{k}=0.86(2\pi/a_0)(1,0,0)$ [22] is small enough to make second-order repulsion between these states non-negligible]. This nonlinearity is related to the splitting of the X_1 state under [110] and [111] stress. Hensel, Hasegawa, and Nakayama[12] have shown that the X_1 splitting and the Δ_1, $\Delta_{2'}$ shifts are given by the Hamiltonian (neglecting hydrostatic contributions)

$$\begin{array}{c} \quad |\Delta_1\rangle \qquad\qquad |\Delta_{2'}\rangle \\ \begin{vmatrix} 0 & 2\mathcal{E}_2^*\epsilon_{xy} \\ 2\mathcal{E}_2^*\epsilon_{yx} & E(\Delta_{2'})-E(\Delta_1) \end{vmatrix} \end{array}\ , \qquad (5)$$

where $\mathcal{E}_2^*$ is a shear-deformation potential.[23]

From Eq. (5), we find for the shift of the Δ_1 conduction-band minima, to second order in stress

$$\delta E^* = -\frac{(2\mathcal{E}_2^*\epsilon_{yx})^2}{E(\Delta_{2'})-E(\Delta_1)}+\cdots\ . \qquad (6)$$

In the above interpretation, terms nonlinear in stress have not been included in the Hamiltonian. Assuming a deformation potential for the nonlinear terms comparable to that for the linear terms (≈ 5 eV) a shift of about 5×10^{-4} eV would be produced at the highest stresses reached in this experiment ($\approx10^{-2}$ strain), and hence these terms are negligible in view of the experimental error in the definition of the exciton energies (± 1 meV). With the exception of the Δ_1–$\Delta_{2'}$ coupling we have neglected any nonlinear effects due to the stress-induced coupling of $\Gamma_{25'}$ or Δ_1 with any other bands since the corresponding gaps are very large.[22]

A. Stress along [111]

For this stress direction, no intervalley splitting of the [001] conduction bands takes place [$\epsilon_{xx}=\epsilon_{yy}=\epsilon_{zz}=(S_{11}+2S_{12})\frac{1}{3}X$]. The splitting of the indirect exciton is due to the splitting of the top $\Gamma_{25'}$ valence-band edge into the bands v_1 and v_2 (see Fig. 1). The spin-orbit split band, which we have labeled v_3, is not shown. The band v_2 is a pure $|\frac{3}{2},\frac{3}{2}\rangle$ state (in the customary spherical notation) while v_1 is mainly $|\frac{3}{2},\frac{1}{2}\rangle$ with a stress-induced admixture of $|\frac{1}{2},\frac{1}{2}\rangle$ (see Appendix A).[5] In addition, there is a quadratic shift of the Δ_1 conduction-band minima given by Eq. (6), where $\epsilon_{xy}=\epsilon_{xz}=\epsilon_{yx}=\frac{1}{6}S_{44}X$.

Taking the valence-band wave functions in the

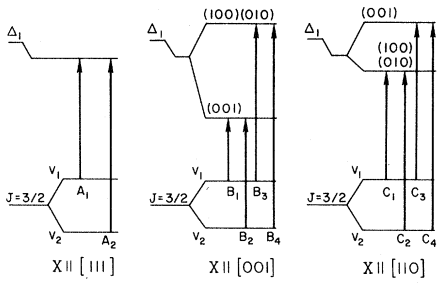

FIG. 1. Schematic representation of the stress-induced splittings of the $\Gamma_{25'}$ valence and Δ_1 conduction bands in silicon. All transitions are allowed for light polarized parallel and perpendicular to the respective stress direction, except the B_2 transition in the case of [001] stress, which is forbidden for the electric field vector of the light perpendicular to the stress axis when one limits the indirect processes to transverse-phonon-assisted transitions only. The spin-orbit split band (v_3) is not shown.

(J, m_J) representation (see Appendix A), the Hamiltonian matrix of Eqs. (1)–(3) becomes

$$\begin{array}{c} \quad |\frac{3}{2},\frac{3}{2}\rangle_{111} \qquad |\frac{3}{2},\frac{1}{2}\rangle_{111} \qquad |\frac{1}{2},\frac{1}{2}\rangle_{111} \\ \begin{vmatrix} -\delta E_H-\frac{1}{2}\delta E_{111} & 0 & 0 \\ 0 & -\delta E_H+\frac{1}{2}\delta E_{111} & \frac{1}{2}\sqrt{2}\delta E'_{111} \\ 0 & \frac{1}{2}\sqrt{2}\delta E'_{111} & -\Delta_0-\delta E'_H \end{vmatrix} \end{array}\ , \qquad (7)$$

where

$$\delta E_H=(a_1+a_2)(S_{11}+2S_{12})X=a(S_{11}+2S_{12})X\ ,$$

$$\delta E'_H=(a_1-2a_2)(S_{11}+2S_{12})X=a'(S_{11}+2S_{12})X\ ,$$

$$\delta E_{111}=\tfrac{1}{3}(\sqrt{3})(d_1+2d_2)S_{44}X=\tfrac{1}{3}\sqrt{3}\,d\,S_{44}X\ ,$$

$$\delta E'_{111}=\tfrac{1}{3}\sqrt{3}(d_1-d_2)S_{44}X=\tfrac{1}{3}\sqrt{3}\,d'\,S_{44}X\ .$$

The S_{11}, S_{12}, and S_{44} are elastic compliance constants whose values are at 77 °K (in units of 10^{-12} dyn^{-1} cm^2)[24]

$$S_{11}=0.863,\quad S_{12}=-0.213,\quad S_{44}=1.249;$$

X is the applied stress, and Δ_0 is the spin-orbit splitting (0.044 eV[25]) in the absence of stress. Diagonalizing the above matrix gives the following expressions for the shift of the v_1 band:

$$\delta E_1^{(111)}=-\tfrac{1}{2}(\bar{\Delta}_0-\tfrac{1}{2}\delta E_{111})-\delta E_H + \tfrac{1}{2}[(\bar{\Delta}_0+\tfrac{1}{2}\delta E_{111})^2+2(\delta E'_{111})^2]^{1/2}, \qquad (8)$$

where

$$\bar{\Delta}_0=\Delta_0-3a_2(S_{11}+2S_{12})X\ , \qquad (9)$$

and for the shift of the v_2 band:

$$\delta E_2^{(111)}=\tfrac{1}{2}\delta E_{111}-\delta E_H\ . \qquad (10)$$

Equations (8) and (10) can be combined to give

$$\delta E_{111}^2 - 2\delta E_{111}(\bar{\Delta}_0 + \tfrac{3}{2}\Delta_{111}) + 2\Delta_{111}(\bar{\Delta}_0 + \Delta_{111}) - (\delta E'_{111})^2 = 0, \tag{11}$$

where $\Delta_{111}(\Delta_{111} = \delta E_1^{(111)} - \delta E_2^{(111)})$ is the measured splitting of the $\Gamma_{25'}$ band. Equation (11) can be rewritten in terms of the deformation potentials d_1, d_2, and a_2 as

$$\{ d_2^2 + 2d_1d_2 + 2\sqrt{3}\,[(S_{11}+2S_{12})/S_{44}](d_1+2d_2)a_2\}(S_{44}X)^2$$
$$-\tfrac{2}{3}\sqrt{3}\,\{(\Delta_0+\tfrac{3}{2}\Delta_{111})(d_1+2d_2)$$
$$+3\sqrt{3}\,[(S_{11}+2S_{12})/S_{44}]\Delta_{111}a_2\}S_{44}X$$
$$+2\Delta_{111}(\Delta_0+\Delta_{111}) \equiv 0. \tag{12}$$

Figure 2 shows the measured stress dependence of the TO-phonon-assisted exciton for stress parallel to [111] with light incident on the [112] face of the sample. As indicated in Fig. 1, A_1 and A_2 represent, respectively, the behavior of the $v_1 \rightarrow \Delta_{1,c}$ and $v_2 \rightarrow \Delta_{1,c}$ indirect transitions. The energy separation between A_1 and A_2 gives the valence-band splitting Δ_{111}.

In the following analysis, we shall neglect a_2.

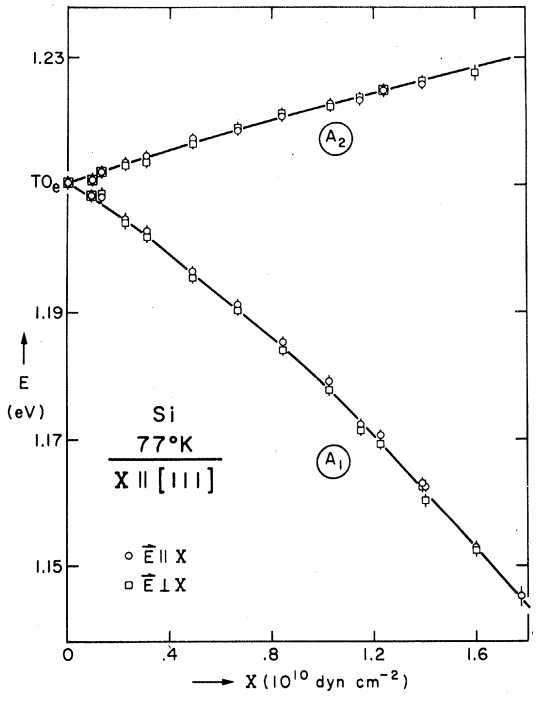

FIG. 2. Effect of [111] stress on the TO-phonon-assisted indirect transition for light polarized parallel and perpendicular to the stress axis and light incident on a $[1\bar{1}2]$ sample face. The energy difference between A_1 and A_2 gives the splitting between the $|v_1\rangle_{111}$ and $|v_2\rangle_{111}$ valence-band states.

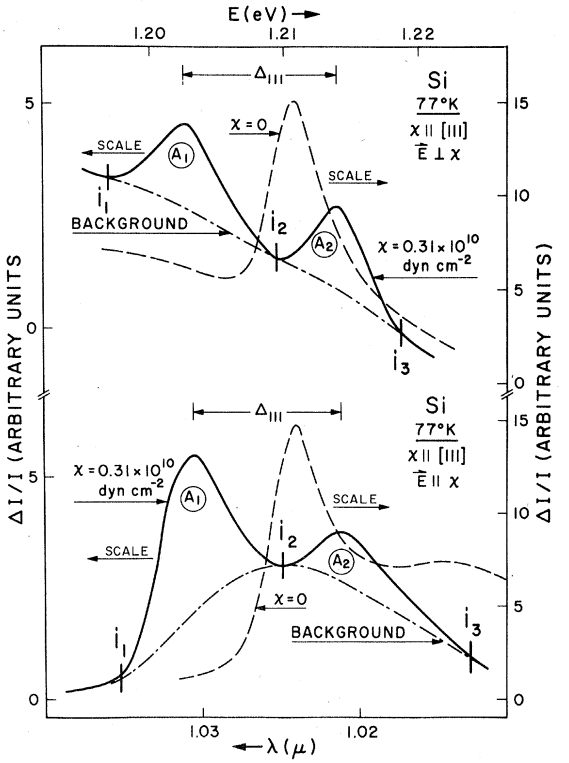

FIG. 3. Spectrum of the indirect transition for zero stress and a [111] stress of 0.31×10^{10} dyn cm^{-2} for light polarized perpendicular and parallel to the stress axis. The zero-stress background is taken to be a smooth line so as to isolate the sharper portions of the structure observed between 1.02 and 1.03 μ for both polarizations. For the stressed case the background is similar in shape to the zero-stress one and follows a smooth line joining the points of the signal labeled i_1, i_2, and i_3 for both polarizations. Relative intensities were obtained by integrating the area between this background and the exciton spectrum.

Brust and Liu[26] have calculated the hydrostatic stress dependence of Δ_0 to be $\delta\Delta_0/\Delta_0 = -4\delta a_0/a_0$. A more detailed calculation using the Korringa-Kohn-Rostoker (KKR) technique[27] yields $\delta\Delta_0/\Delta_0 = -1.3\delta a_0/a_0$, so that

$$a_2 = \tfrac{1.3}{9}\Delta_0 . \tag{13}$$

Since for Si, $\Delta_0 = 0.044$ eV, $a_2 = 0.006$ eV; as we shall see later this value can be neglected in view of the much larger error in our determination of deformation potentials.

At stresses below 6×10^9 dyn cm^{-2} the quadratic term in Eq. (12) can be neglected and hence

$$\delta E_{111} = \Delta_{111}(\Delta_0+\Delta_{111})/(\Delta_0+\tfrac{3}{2}\Delta_{111}). \tag{14}$$

From the experimental values of Δ_{111} and Δ_0 we find $d = d_1 + 2d_2 = -(4.85 \pm 0.15)$ eV. Once a value of d has been obtained, the results at $X > 6\times10^9$

dyn cm^{-2} are used with Eq. (12) to obtain $d_1 = -(4.90 \pm 0.25)$ eV and $d_2 = -(0.05 \pm 0.25)$ eV. Independent values of d_1 and d_2 have not been reported before for silicon, although they have been measured in germanium.[28] However, Balslev[4] found $-(5.3 \pm 0.4)$ eV for d; the marginal discrepancy between this result and ours is probably related to the fact that the A_2 branch, as observed by Balslev, exhibits a nonlinear shift to higher energies which cannot be explained theoretically. Cyclotron resonance measurements[2] yield $d = -3.1$ eV, while values of -4.8 (Ref. 29) and -5.1 (Ref. 30) eV were derived by calculating the bands of the stressed material. A recently published work[13] gives $d = -4.9$ eV, which agrees very well with our measurement.

The quadratic shift of $\Delta_{1,c}$ affects both lines A_1 and A_2. From Eqs. (6) and (10), the nonlinearity affecting A_2 is connected with the stress-induced $\{\Delta_1; \Delta_{2'}\}$ coupling in the conduction band. We have determined the corresponding deformation potential $\mathcal{E}_2^*$ from a quadratic fit of A_2 in Fig. 2, which yields $|\mathcal{E}_2^*| = (7.5 \pm 2)$ eV [according to Eq. (6) only the magnitude of $\mathcal{E}_2^*$ can be determined from our data]. The hydrostatic deformation potential $\mathcal{E}_1 + a_1$ can also be evaluated from the A_2 branch [see Eq. (10)] which gives $\mathcal{E}_1 + a_1 = +(1.5 \pm 0.3)$ eV. The above values of the deformation potentials give a good fit to the stress dependence of the A_1 line. The values of $\mathcal{E}_1 + a_1$ are in good agreement with hydrostatic pressure measurements[31-33] and are in contrast to the high values of this quantity determined by other workers with uniaxial stress.[4,13]

Shown in Fig. 3 is the spectrum of the indirect transition for zero stress and a [111] stress of 0.31×10^{10} dyn cm^{-2} for light polarized perpendicular and parallel to the stress axis. The background was determined from the zero-stress spectrum. The signal outside the range $1.02\mu < \lambda < 1.03\mu$ at zero stress is taken to be background. For the stressed case the zero-stress background signal has been displaced to correspond to the displacement of the peaks. The experimental values of the intensities were obtained by integrating the exciton peaks above the background.

The measured intensities of the A_1 and A_2 lines, at 0.31×10^{10} dyn cm^{-2}, are reported in Table I, together with theoretical values assuming one ($\Gamma_{15,c}$ or $\Delta_{5,v}$) or two ($\Gamma_{15,c}$ and $\Delta_{5,v}$) intermediate states, as derived from the theoretical expressions given in Appendix B and Table II. At this value of stress the two branches are already resolved but not yet seriously affected by changes in linewidth associated with changes in the elastic scattering probability (density of final states) induced by the splitting. For light polarized parallel to [111], adding the $\Delta_{5,v}$ contribution to the single indirect mechanism through $\Gamma_{15,c}$ improves the fit of the observed intensities. However, for the light polarized perpendicular to [111], none of the proposed mechanisms seem to be satisfactory: The A_1 line is observed stronger than the A_2 line.

TABLE I. Theoretical and experimental values of the intensities of indirect transitions in silicon at low stresses and for different light polarizations. The experimental values were obtained by integrating the exciton peaks above the background signal in the recorded spectra at stresses for which the different exciton branches are already resolved but not yet seriously affected by differences in the elastic scattering of electrons induced by the stress. The theoretical evaluations are given for one ($\Gamma_{15,c}$ or $\Delta_{5,v}$) or two ($\Gamma_{15,c}$ and $\Delta_{5,v}$) intermediate states; they derive from equations given in Appendix B and Table II. The theoretical intensities calculated for the superposition of two intermediate states take account of the different energy denominators attributed to each single mechanism: $\{[E(\Delta_{1,c}) - E(\Gamma_{15,c})]/[E(\Gamma_{25',v}) - E(\Delta_{5,v})]\}^2 \approx \frac{5}{8}$ (see Appendix B). Matrix elements have been taken equal in both cases.

Intermediate states		Theoretical relative intensities									Observed relative intensities		
		$\Gamma_{15,c}$			$\Delta_{5,v}$			$\Gamma_{15,c}$ and $\Delta_{5,v}$					
	$\vec{E}\parallel$	[111]	[11$\bar{2}$]		[111]	[11$\bar{2}$]		[111]	[11$\bar{2}$]		[111]	[11$\bar{2}$]	
$X\parallel$[111]	A_1	77	39		53	50		68	43		68	58	
($X = 0.31 \times 10^{10}$ dyn cm^{-2})	A_2	23	61		47	50		32	57		32	42	
	$\vec{E}\parallel$	[001]	[110]		[001]	[110]		[001]	[110]		[001]	[110]	
$X\parallel$[001]	B_1	7	30		0	31		4	31		≈ 0	69	
($X = 0.33 \times 10^{10}$ dyn cm^{-2})	B_2	43	0		0	0		26	0		20	0	
	B_3	7	35		14	20		10	29		18	18	
	B_4	43	35		86	46		60	40		62	13	
	$\vec{E}\parallel$	[110]	[1$\bar{1}$0]	[001]	[110]	[1$\bar{1}$0]	[001]	[110]	[1$\bar{1}$0]	[001]	[110]	[1$\bar{1}$0]	[001]
$X\parallel$[110]	C_1	56	19	31	32	32	62	47	25	44	48	27	50
($X = 0.26 \times 10^{10}$ dyn cm^{-2})	C_2	19	56	19	19	19	38	19	41	27 / 18	27	50	50
	C_3	6	6	31	12	12	0	8	9				
	C_4	19	19	19	37	37	0	26	25	11	25	23	≈ 0

TABLE II. Theoretical expressions of the intensities of indirect transitions in silicon as a function of stress, assuming one ($\Gamma_{15,c}$ or $\Delta_{5,v}$) or two ($\Gamma_{15,c}$ and $\Delta_{5,v}$) intermediate states.

Intermediate state		$\Gamma_{15,c}$		$\Delta_{5,v}$		$\Gamma_{15,c}$ and $\Delta_{5,v}$	
	$\vec{E}\parallel$	[111]	[11$\bar{2}$]	[111]	[11$\bar{2}$]	[111]	[11$\bar{2}$]
$X\parallel$[111]	A_1	$\frac{3}{4}\eta_1^1$	$\frac{3}{8}\eta_3^1$	$\frac{1}{2}\eta_2^1$	$\frac{1}{2}\eta_4^1$	$\frac{6}{13}\eta_1^1+\frac{5}{26}\eta_2^1$	$\frac{3}{13}\eta_3^1+\frac{5}{26}\eta_4^1$
	A_2	$\frac{1}{4}$	$\frac{5}{8}$	$\frac{1}{2}$	$\frac{1}{2}$	$\frac{9}{26}$	$\frac{15}{26}$
	$\vec{E}\parallel$	[001]	[110]	[001]	[110]	[001]	[110]
$X\parallel$[001]	B_1	$\frac{1}{8}\eta_1^0$	$\frac{1}{4}\eta_2^0$	0	$\frac{1}{2}\eta_2^0$	$\frac{1}{13}\eta_1^0$	$\frac{9}{26}\eta_2^0$
	B_2	$\frac{3}{8}$	0	0	0	$\frac{3}{13}$	0
	B_3	$\frac{1}{8}\eta_1^0$	$\frac{3}{8}$	$\frac{1}{4}\eta_1^0$	$\frac{1}{8}\eta_1^0$	$\frac{9}{52}\eta_1^0$	$\frac{3}{13}+\frac{5}{104}\eta_1^0$
	B_4	$\frac{3}{8}$	$\frac{3}{8}$	$\frac{3}{4}$	$\frac{3}{8}$	$\frac{27}{52}$	$\frac{39}{104}$

	$\vec{E}\parallel$	[110]	[1$\bar{1}$0]	[001]	[110]	[1$\bar{1}$0]	[001]	[110]	[1$\bar{1}$0]	[001]
$X\parallel$[110]	C_1	$\frac{1}{16}(\eta_{11}^2+4\eta_{13}^2)$	$\frac{1}{16}(\eta_{11}^2+4\eta_{12}^2)$	$\frac{1}{8}(\eta_{12}^2+\eta_{13}^2)$	$\frac{1}{8}(\eta_{12}^2+\eta_{13}^2)$	$\frac{1}{8}(\eta_{12}^2+\eta_{13}^2)$	$\frac{1}{4}(\eta_{12}^2+\eta_{13}^2)$	$\frac{1}{16}\eta_{11}^2+\frac{5}{64}\eta_{12}^2+\frac{21}{64}\eta_{13}^2$	$\frac{1}{16}\eta_{11}^2+\frac{5}{64}\eta_{13}^2+\frac{21}{64}\eta_{12}^2$	$\frac{9}{32}(\eta_{12}^2+\eta_{13}^2)$
	C_2	$\frac{1}{16}(\eta_{21}^2+4\eta_{23}^2)$	$\frac{1}{16}(\eta_{21}^2+4\eta_{22}^2)$	$\frac{1}{8}(\eta_{22}^2+\eta_{23}^2)$	$\frac{1}{8}(\eta_{22}^2+\eta_{23}^2)$	$\frac{1}{8}(\eta_{22}^2+\eta_{23}^2)$	$\frac{1}{4}(\eta_{22}^2+\eta_{23}^2)$	$\frac{1}{16}\eta_{21}^2+\frac{5}{64}\eta_{22}^2+\frac{21}{64}\eta_{23}^2$	$\frac{1}{16}\eta_{21}^2+\frac{5}{64}\eta_{23}^2+\frac{21}{64}\eta_{22}^2$	$\frac{9}{32}(\eta_{22}^2+\eta_{23}^2)$
	C_3	$\frac{1}{16}\eta_{11}^2$	$\frac{1}{16}\eta_{11}^2$	$\frac{1}{8}(\eta_{12}^2+\eta_{13}^2)$	$\frac{1}{8}\eta_{11}^2$	$\frac{1}{8}\eta_{11}^2$	0	$\frac{9}{64}\eta_{11}^2$	$\frac{9}{64}\eta_{11}^2$	$\frac{1}{8}(\eta_{12}^2+\eta_{13}^2)$
	C_4	$\frac{1}{16}\eta_{21}^2$	$\frac{1}{16}\eta_{21}^2$	$\frac{1}{8}(\eta_{22}^2+\eta_{23}^2)$	$\frac{1}{8}\eta_{21}^2$	$\frac{1}{8}\eta_{21}^2$	0	$\frac{9}{64}\eta_{21}^2$	$\frac{9}{64}\eta_{21}^2$	$\frac{1}{8}(\eta_{22}^2+\eta_{23}^2)$

$\eta_1^1=[n_1(n_1-m_1)]^{-1}\,[\frac{1}{3}(n_1-m_1)^2+\frac{8}{9}(n_1-m_1)\,\delta E'_{111}+(\delta E'_{111})^2]$, $\eta_2^1=[n_1(n_1-m_1)]^{-1}\,[\frac{1}{2}(n_1-m_1)^2+\frac{2}{3}(n_1-m_1)\,\delta E'_{111}+(\delta E'_{111})^2]$,

$\eta_3^1=[n_1(n_1-m_1)]^{-1}\,[\frac{2}{3}(n_1-m_1)^2+\frac{2}{9}(n_1-m_1)\,\delta E'_{111}+(\delta E'_{111})^2]$, $\eta_4^1=[n_1(n_1-m_1)]^{-1}\,[\frac{1}{2}(n_1-m_1)^2+\frac{5}{6}(n_1-m_1)\,\delta E'_{111}+(\delta E'_{111})^2]$,

$\eta_1^0=[n_0(n_0-m_0)]^{-1}\,[(n_0-m_0)-\delta E'_{001}]^2$, $\eta_2^0=[n_0(n_0-m_0)]^{-1}\,[\frac{1}{2}(n_0-m_0)+\delta E'_{001}]^2$,

(all these quantities are equal to unity at zero stress);

$\eta_{11}^2=\frac{1}{6}(\sqrt{3}\gamma_{12}-\gamma_{11}+\sqrt{2}\gamma_{13})^2$, $\eta_{12}^2=\frac{1}{12}(\sqrt{3}\gamma_{12}+\gamma_{11}-\sqrt{2}\gamma_{13})^2$, $\eta_{13}^2=\frac{1}{6}(\sqrt{2}\gamma_{11}+\gamma_{13})^2$,

$\eta_{21}^2=\frac{1}{6}(\sqrt{3}\gamma_{22}-\gamma_{21}+\sqrt{2}\gamma_{23})^2$, $\eta_{22}^2=\frac{1}{12}(\sqrt{3}\gamma_{22}+\gamma_{21}-\sqrt{2}\gamma_{23})^2$, $\eta_{23}^2=\frac{1}{6}(\sqrt{2}\gamma_{21}+\gamma_{23})^2$.

At $X=0$:

$\eta_{11}^2=1$, $\eta_{12}^2=\frac{1}{2}$, $\eta_{13}^2=2$, $\eta_{21}^2=3$, $\eta_{22}^2=\frac{3}{2}$, $\eta_{23}^2=0$.

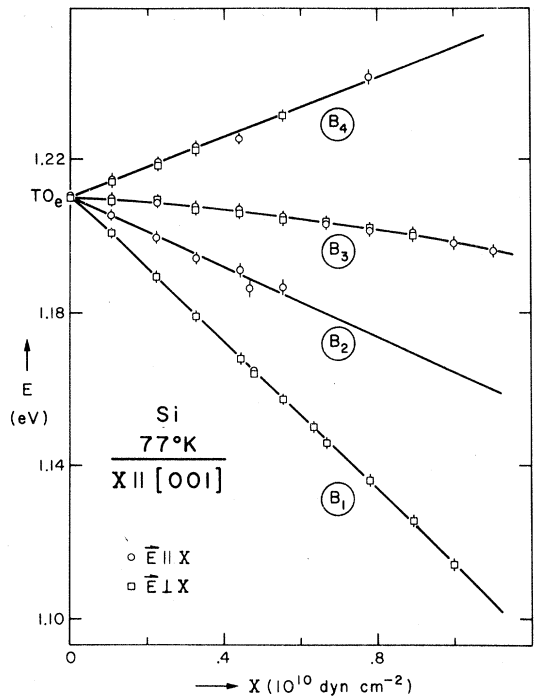

FIG. 4. Stress dependence of the TO-phonon-assisted indirect transition for [001] stress with light polarized parallel and perpendicular to the stress axis and light incident on a [1$\bar{1}$0] sample face. The B_1 and B_2 lines correspond to transitions from the $|v_1\rangle_{001}$ valence band to the $\Delta_{1,c}$ singlet ([001] valley) and doublet ([010] and [100] valleys), respectively, while B_2 and B_4 correspond to transitions from $|v_2\rangle_{001}$ to the singlet and doublet, respectively.

B. Stress along [001]

A [001] stress does not split the Δ_1 and $\Delta_{2'}$ conduction-band degeneracy at X_1 and hence there is no quadratic shift of the Δ_1 bands ($\epsilon_{xz} = \epsilon_{yz} = \epsilon_{yx} = 0$). However, the six Δ_1 minima are no longer equivalent, resulting in an intervalley splitting described by the shear deformation potential $\mathcal{E}_2$. Along the [001] valley, the Δ_1 shift is

$$\delta E_{1,c}^{(001)} = -\tfrac{2}{3}\mathcal{E}_2(S_{11} - S_{12})X \quad \text{(singlet)} \tag{15}$$

and along the [010] and [100] valleys

$$\delta E_{2,c}^{(100)} = \tfrac{1}{3}\mathcal{E}_2(S_{11} - S_{12})X \quad \text{(doublet)}. \tag{16}$$

This situation is shown schematically in Fig. 1.

Here again the degeneracy of $\Gamma_{25'}$ is lifted producing two levels v_1 and v_2. For this stress direction the Hamiltonian matrix of Eq. (7) is similar to that given in the [111] case, with δE_{111} and $\delta E'_{111}$ replaced by $\delta E_{001} = 2(b_1 + 2b_2)(S_{11} - S_{12})X$, and $\delta E'_{001} = 2(b_1 - b_2)(S_{11} - S_{12})X$, respectively. The same substitution applies to Eqs. (8)-(12) and (14), which now give the shifts $\delta E_1^{(001)}$ and $\delta E_2^{(001)}$ of the v_1 and v_2 bands, and their sum Δ_{001} which represents the experimental $(v_1; v_2)$ splitting in the presence of a [001] stress. The stress dependence of the TO-phonon-assisted transition for [001] stress is shown in Fig. 4. Light was incident on a [110] sample face. The labeling of the four branches is shown in Fig. 1. This figure also indicates that the splitting Δ_{001} can be evaluated from the energy separation of both $(B_1 - B_2)$ and $(B_3 - B_4)$. From the data of Fig. 3 and an analysis similar to that for [111] stress we find $b = -(2.10 \pm 0.10)$ eV, $b_1 = -(1.95 \pm 0.15)$ eV, and $b_2 = -(0.10 \pm 0.15)$ eV. The corresponding value of $\mathcal{E}_1 + a_1$ is found to be $+2.0 \pm 1.0$ eV. The value found here for $b = b_1 + 2b_2$ is in reasonable agreement with earlier experimental results.[2,4,13] Theoretical calculations give $b = -2.5$ eV[29] and $b = -2.0$ eV.[30] Although the value of $\mathcal{E}_1 + a_1$ determined from these [001] data is higher than the value measured for [111] stress, the accuracy in this case is lower than in the previous case. This is due partly to the conduction-band splitting along Δ_1, which introduces new sources of error, and partly to electron scattering in the valence band, which increases the widths of excitons associated with v_2 and makes difficult the determination of the B_2 and B_4 branches at stresses higher than approximately 0.5×10^{10} dyn cm^{-2}.

The intervalley splitting of Δ_1 can be determined from the separation of $(B_1 - B_3)$ and $(B_2 - B_4)$. The corresponding shear deformation potential is $\mathcal{E}_2 = -(8.7 \pm 0.4)$eV, which is in good agreement with other work.[4]

The experimental strengths of the observed peaks are shown in Table I for stress of 0.33×10^{19} dyn cm^{-2}, compared with theoretical values (see Appendix B and Table II). For light polarized parallel to [001], calculations assuming only one intermediate state ($\Gamma_{15,c}$) are not sufficient to explain the measured relative intensities of the B_2 and B_4 lines, since the calculated strengths would be equal while the calculated B_4 is a factor of 3 more intense than B_2 (see Table I). However, if we add the indirect process through the $\Delta_{5,v}$ valence band to our interpretation, then these theoretical intensities are well differentiated, in good agreement with the experimental features. This provides strong evidence for the contributions of $\Delta_{5,v} \rightarrow \Delta_{1,c}$ virtual transitions to the observed indirect excitons. For the other polarization, the B_1 line was found to be the strongest; none of the proposed processes is able to account for this fact. This discrepancy is not understood. Intensity measurements performed at 0.11×10^{10} dyn cm^{-2} have shown results closer to the theoretical estimates, which might indicate that the v_2 level, from which the B_4 strong transition originates, is quickly broadening through scattering mechanisms when stresses are applied. However, this effect does not seem sufficient to explain the discrepancy completely.

C. Stress along [110]

For the case of stress parallel to [001] or [111] the choice of the quantization axis along the stress direction led to a simple form for the Hamiltonian and the wave functions. This choice preserved m_J as a good quantum number and hence led to well defined selection rules and an easy identification of states. However, when stress is applied to an axis of lower symmetry, such as the [110] axis, the situation is more complex. For stress parallel to [001] or [111] the crystal is uniaxial and hence the intensities of the transitions are independent of the azimuthal angle of the incident radiation about the stress axis. However, this is not the case for stress parallel to [110] since, as is shown below, m_J is no longer a good quantum number, i.e., the [110] stress couples the v_2 band to the v_1 and v_3 bands. The crystal is biaxial and the intensities of the various transitions will depend on the azimuthal angle of the incident radiation.

Using the wave functions referred to the [110] axis as the z axis, as given in Appendix A, the Hamiltonian matrix of Eqs. (1)-(3) for this stress direction can be written as follows:

$$\begin{array}{c} \left|\tfrac{3}{2},\tfrac{3}{2}\right\rangle_{110} \quad \left|\tfrac{3}{2},-\tfrac{1}{2}\right\rangle_{110} \quad \left|\tfrac{1}{2},-\tfrac{1}{2}\right\rangle_{110} \\ \begin{vmatrix} -\frac{1}{2}\delta E_{110}-\delta E_H & -\frac{1}{8}\sqrt{3}\,\delta\epsilon & \frac{1}{8}\sqrt{6}\,\delta\epsilon' \\ -\frac{1}{8}\sqrt{3}\,\delta\epsilon & \frac{1}{2}\delta E_{110}-\delta E_H & \frac{1}{2}\sqrt{2}\,\delta E'_{110} \\ \frac{1}{8}(\sqrt{6})\delta\epsilon' & \frac{1}{2}\sqrt{2}\,\delta E'_{110} & -\Delta_0-\delta E'_H \end{vmatrix} \end{array} , \tag{17}$$

where

$$\delta E_{110}=\tfrac{1}{4}(\delta E_{001}+3\delta E_{111}),\quad \delta E'_{110}=\tfrac{1}{4}(\delta E'_{001}+3\delta E'_{111}),$$

$$\delta\epsilon=(\delta E_{001}-\delta E_{111}),\qquad \delta\epsilon'=(\delta E'_{001}-\delta E'_{111}).$$

In the case that $\delta E_{001}=\delta E_{111}$ and $\delta E'_{001}=\delta E'_{111}$ (equal valence-band splitting under applied stress along [001] or [111]) the above matrix would have the same form as Eq. (7). In fact, under this condition the valence-band splitting becomes isotropic and the Hamiltonian matrix has the form of Eq. (7) for any stress direction. From the [111] and [001] data, it may be noted that the quantities $\delta\epsilon$ and $\delta\epsilon'$ are small compared to δE_{110} and $\delta E'_{110}$ and can be neglected to first order in $\delta\epsilon/\delta E_{110}$ (numerator and denominator either primed or unprimed). The eigenvalues of Eq. (17) can then be obtained by diagonalizing the 2×2 matrix in the lower right-hand corner and introducing the effects of the $\{v_1, v_2\}$ and $\{v_3, v_2\}$ couplings by second-order perturbation theory. In this manner the following energies are obtained: for the v_1 level

$$\delta E_1=-\tfrac{1}{2}(\bar{\Delta}_0-\tfrac{1}{2}\delta E_{110})-\delta E_H+\tfrac{1}{2}n_2+W_1^2, \tag{18}$$

where

$$W_1^2=\frac{3}{16}\frac{1}{q_2^2}\frac{[\delta E'_{110}\delta\epsilon-(n_2-m_2)\delta\epsilon']^2}{2\delta E_{110}+(n_2-m_2)};$$

for the v_2 level

$$\delta E_2=-\tfrac{1}{2}\delta E_{110}-\delta E_H+W_2^2, \tag{19}$$

where

$$W_2^2=-\frac{3}{16}\frac{1}{q_2^2}\frac{[\delta E'_{110}\delta\epsilon-(n_2-m_2)\delta\epsilon']^2}{2\delta E_{110}+(n_2-m_2)}$$

$$-\frac{3}{32}\frac{1}{q_2^2}\frac{[2\delta E'_{110}\delta\epsilon'+(n_2-m_2)\delta\epsilon]^2}{2\delta E_{110}-(m_2+n_2)};$$

for the v_3 level

$$\delta E_3=-\tfrac{1}{2}(\bar{\Delta}_0-\tfrac{1}{2}\delta E_{110})-\delta E_H-\tfrac{1}{2}n_2+W_3^2, \tag{20}$$

where

$$W_3^2=+\frac{3}{32}\frac{1}{q_2^2}\frac{[2\delta E'_{110}\delta\epsilon'+(n_2-m_2)\delta\epsilon]^2}{2\delta E_{110}-(m_2+n_2)},$$

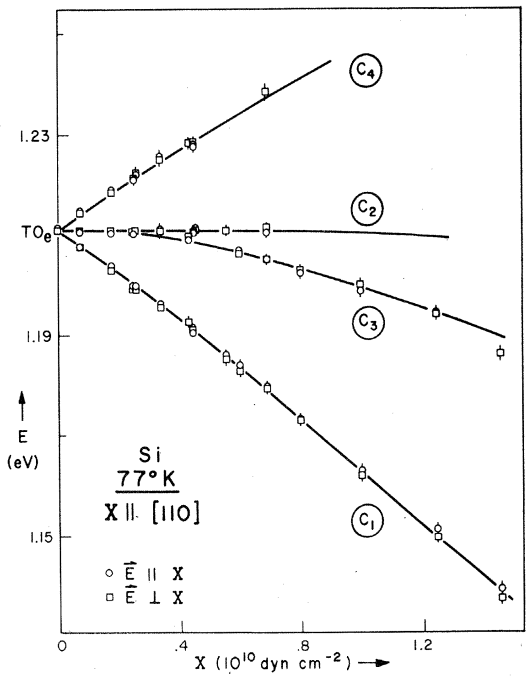

FIG. 5. Stress dependence of the TO-phonon-assisted transitions for [110] stress with light polarized parallel and perpendicular to the stress axis. Measurements were made on samples with light incident on [001] and [110] faces. The C_1, and C_3 lines correspond to transitions from $|v_1\rangle_{110}$ to the $\Delta_{1,c}$ doublet and singlet, respectively, while C_2 and C_4 correspond to transitions from $|v_2\rangle_{110}$ to the doublet and singlet, respectively.

with

$$m_2 = \bar{\Delta}_0 + \tfrac{1}{2}\delta E_{110}, \quad n_2 = [m_2^2 + 2(\delta E'_{110})^2]^{1/2},$$
$$q_2^2 = 2n_2(n_2 - m_2). \tag{21}$$

The conduction-band behavior under [110] stress is more complicated than for the other stress directions. First, a [110] stress induces an intravalley splitting at the X point, which results in a quadratic shift of the Δ_1 band [Eqs. (5) and (6)] only along the [001] valley ($\epsilon_{yx} = \frac{1}{4}S_{44}X$), leaving unaffected the other two equivalent valleys [010] and [100] ($\epsilon_{xz} = \epsilon_{yz} = 0$). In addition, there is an intervalley splitting of Δ_1 as shown in Fig. 1, which results in another segregation of the valleys. The shift of Δ_1 in this case is given by, to second order in stress

$$\delta E_{1,c}^{(110)} = \tfrac{1}{3}\mathcal{E}_2(S_{11} - S_{12})X + \delta E^* \quad \text{(singlet)}$$
$$\text{for the [001] valley} \tag{22}$$

and

$$\delta E_{2,c}^{(110)} = -\tfrac{1}{6}\mathcal{E}_2(S_{11} - S_{12})X \text{ (doublet)}$$
$$\text{for the [010] and [100] valleys}. \tag{23}$$

The linear splitting of the Δ_1 band for a [110] stress is then found to be half of the Δ_1 splitting under a [001] stress of the same magnitude and inverted, the doublet being shifted to lower energy and not to higher energy as for a [001] stress.

The observed behavior of the TO excitons in the presence of a [110] stress is shown in Fig. 5. Measurements were made on samples with light incident on both [001] and [1$\bar{1}$0] faces. The four branches labeled C_1, C_2, C_3, and C_4 correspond to transitions shown in Fig. 1. The C_2 line is observed taking the electric field of the incident light parallel to the [1$\bar{1}$0] crystal axis ($\vec{E} \perp$ [110] with [001] incident face). Elastic scattering in the valence band obscures this line above about 0.7×10^{10} dyn cm^{-2}, while the C_3 line is barely observable for this polarization in agreement with theoretically computed intensities, as shown in Table I. For the electric field polarized parallel to [001] ($\vec{E} \perp$ [110] and [1$\bar{1}$0] incident face), the C_2 line is not observed at high stresses, unlike the C_3 line which remains strong up to 1.4×10^{10} dyn cm^{-2}. For the third light polarization ($\vec{E} \parallel$ [110]), both lines are observed although the C_2 line disappears again at about 0.7×10^{10} dyn cm^{-2} for the reason mentioned above. The C_1 line is clearly observed for the three light polarizations. The C_3 branch should exhibit the strongest nonlinearity. It involves transitions originating at v_1 whose quadratic shift according to Eq. (18) is considerably larger than the v_2 shift given by Eq. (19). Moreover, the final state of these C_3 transitions is the singlet in Δ_1 which is affected by the $\{\Delta_1, \Delta_{2'}\}$ coupling (quadratic shift). In contrast, the C_2 line is expected to be almost linear; the corresponding transitions originate in v_2 and end on the doublet which does not couple with $\Delta_{2'}$. From that comparison, the C_2 and C_3 lines should be strongly differentiated at high stresses. Up to approximately $(0.4-0.5)\times10^{10}$ dyn cm^{-2}, Fig. 4 shows that the two lines are not resolved, which indicates nearly equal splittings of $\Gamma_{25',v}$ and $\Delta_{1,c}$ as observed by Balslev.[4] Increasing the stress above that value makes the two lines clearly distinct.

In order to clarify our understanding of these data, we computed the theoretical intensities of the indirect transitions between $\Gamma_{25',v}$ and $\Delta_{1,c}$ assuming one ($\Gamma_{15,c}$ or $\Delta_{5,v}$) or two ($\Gamma_{15,c}$ and $\Delta_{5,v}$) intermediate states, as for the other stress directions. The results are compared in Table I with the measured intensities at 0.26×10^{10} dyn cm^{-2}. For this stress, the C_2 and C_3 transitions are degenerate and we only consider the sum of their intensities. For $\vec{E} \parallel$ [110], the fit to the experimental data is slightly better when adding the Δ_5 intermediate state contribution to $\Gamma_{15,c}$ than when considering $\Gamma_{15,c}$ alone. For $E \parallel$ [001], the C_4 line was practically unobservable, which is in better agreement with the double mechanism than with the single one (via $\Gamma_{15,c}$); for this single intermediate state the C_4 line should be about 40% of the $(C_2 + C_3)$ line. Also, the C_1 and $(C_2 + C_3)$ lines have equal intensity, in agreement with the double mechanism. In the case where $\vec{E}$ is parallel to [110], the C_4 line was well resolved and its intensity evaluated, though the same line was not observed for $\vec{E} \parallel$ [001]; this difference can only be interpreted through the double mechanism: The single mechanism assigns the same intensity to this line for both polarizations.

The observed preponderance of C_2 over C_3 for $\vec{E} \parallel$ [110] is well explained through both single and double mechanisms. When $\vec{E}$ is parallel to [001] however, C_3 is found to be increasingly stronger than C_2. The single mechanism would explain such behavior better than the double mechanism. A possible way to reconcile this fact with our previous conclusions may be found in the broadening by elastic scattering. Such broadening would have to be stronger for C_2 than for the C_3 line. This would require a broadening of the v_2 band due to the overlapping density of v_1 states after splitting.

For this stress direction the singlet-doublet conduction-band splitting can be evaluated from the $(C_1 - C_3)$ and $(C_2 - C_4)$ separation [see Figs. 1 and 5 and Eqs. (22) and (23)]. By fitting the stress dependence of the energy separation of these lines to an expression quadratic in the stress, we find $\mathcal{E}_2 = -(8.5 \pm 0.5)$ eV and $|\mathcal{E}_2^*| = (9 \pm 3)$ eV, in good agreement with the [001] and [111] stress data.

It can be shown that the terms W_i^2 $(i = 1, 2, 3)$ in

TABLE III. Deformation potentials of the $\Gamma_{25'}$ valence and Δ_1 conduction bands of silicon obtained in this and in previously published work.

Stress direction	This work [111]	This work [011]	This work [110]	Previous works	Ref.
d (eV)	-4.85 ± 0.15			$d=-5.3\pm0.4$	4
d_1 (eV)	-4.90 ± 0.25			$d=-3.1$	2
d_2 (eV)	-0.05 ± 0.25			$d=-4.9$	13
				$d=-4.8$	29
				$d=-5.1$	30
b (eV)		-2.10 ± 0.10		$b=-2.4\pm0.2$	4
b_1 (eV) 1		-1.95 ± 0.15		$b=-1.4$	2
b_2 (eV)		-0.10 ± 0.15		$b=-2.1$	13
				$b=-2.5$	29
				$b=2.0$	30
$\delta E_{110}/X$ (10^{12} eV cm^2 dyn^{-1})			3.9 ± 0.2		
$\delta E'_{110}/X$ (10^{-12} eV cm^2 dyn^{-1})			3.7 ± 0.5		
$\mathcal{E}_1+a_1$ (eV)	$+1.5\pm0.3$	$+2.0\pm0.0$	$+1.7\pm0.6$	$\mathcal{E}_1+a_1=+4.3\pm0.5$	4
				$=+4.4$	13
				$=+1.5$	31
				$=+1.8\pm0.3$	33
$\mathcal{E}_1$ (eV)		-8.7 ± 0.4	-8.5 ± 0.5	$\mathcal{E}_2=-8.6\pm0.2$	4
				$=-8.0\pm1$	13
				$=-9.5$	29
$\lvert\mathcal{E}_2'\rvert$ (eV)	$7.5^{(+)}\pm2$		$9^{(+)}\pm3$	$\lvert\mathcal{E}_2'\rvert = 9\pm1$[a]	12
				$= 7.8$	29
				$= 7.5$	30

Eqs. (18)–(20) can be neglected (using the values of b_1, b_2, d_1, and d_2 listed in Table III). Under these conditions, Eqs. (18) and (19) are analogous to Eqs. (8) and (10), and hence it is possible to evaluate δE_{110} and $\delta E'_{110}$ in a manner similar to that used to obtain the corresponding parameters for [001] and [111] stress. The values of $\delta E_{110}/X=\frac{1}{4}[2b(S_{11}-S_{12})+\sqrt{3}dS_{44}]$ and $\delta E'_{110}/X=\frac{1}{4}[2b'(S_{11}-S_{12})+\sqrt{3}d'S_{44}]$ are listed in Table III; they are consistent with the values of b, b', d, and d' obtained from the other stress direction measurements. From the stress dependence of the C_2 line and the values of δE_{110} and $\mathcal{E}_2$ a value of $\mathcal{E}_1+a_1=+(1.7\pm0.6)$ eV has been determined. We find that the above values of the deformation potentials and the quantities $\delta E_{110}/X$ and $\delta E'_{110}/X$ give a good fit to the stress dependence of the C_1, C_3, and C_4 lines.

IV. RESULTS AND CONCLUSIONS

The results for the deformation potentials obtained in this work are summarized in Table III together with previous results. Because of the high stresses reached in our experiment we have been able to measure accurately the nonlinearities in the stress dependence of the TO-phonon-assisted indirect transition. This has enabled us to determine independently the valence-band deformation potentials associated with the orbital-strain interaction (b_1 and d_1) and the spin-orbit-strain interaction (b_2 and d_2). The fact that we have been able to fit the data without using a_2 justifies our original assumption that $a_2=0$. The quantities $b=(b_1+2b_2)$ and $d=(d_1+2d_2)$ are in good agreement with earlier works by Balslev[4] and Akimchenko and Vdovenkov,[12] although our accuracy is somewhat better. Our value of the dydrostatic pressure coefficient $(\mathcal{E}_1+a_1)$ is in sharp disagreement with their values but agrees quite well with values obtained from measurements under hydrostatic pressure[31]:

$$\left(\frac{\delta E}{\delta P}\right)_i = -3(S_{11}+2S_{12})(\mathcal{E}_1+a_1)$$

$$= -1.5\times10^{-12}\ \text{eV dyn}^{-1}\,\text{cm}^2\,, \qquad (24)$$

while our value of $(\delta E/\delta P)_i=-(1.8\pm0.5)\times10^{-2}$ eV dyn^{-1} cm^2. Warschauer and Paul[32] report $(\delta E/\delta P)_i=-1.3\times10^{-12}$ eV dyn^{-1} cm^2. Nathan and Paul[33] have studied the effects of hydrostatic pressure on the indirect gap by measuring the change in resistivity of gold-doped silicon with pressure. They find $(\delta E/\delta P)_i=-(1.5\pm0.3)\times10^{-12}$ eV dyn^{-1} cm^2 in the range $(0-4)\times10^{10}$ dyn cm^{-2}, and $-(2.4\pm0.3)\times10^{-12}$ eV dyn^{-1} cm^2 at 2.0×10^{10} dyn cm^{-2}. It should be noted that the technique used for applying uniaxial stress and measuring the exciton spectrum in this work was the

same as that used previously in AlSb[15] and in GaP[34] for which there is a serious discrepancy between uniaxial and hydrostatic data.

On the basis of the point-ion model Suzuki and Hensel[8] have calculated the following expressions for b_2 and d_2:

$$b_2 = -\tfrac{1}{9}\Delta_0\,, \qquad d_2 = -\tfrac{1}{9}\sqrt{3}\,\Delta_0\,. \tag{25}$$

Our experimental values for these parameters are not inconsistent with the predictions of this model ($b_2 = -0.005$ eV and $d_2 = -0.0085$ eV), although a detailed comparison cannot be made because of our large experimental error. Hensel and Suzuki[28] have determined values of $b_2 = -(0.22 \pm 0.02)$ eV and $d_2 = -(0.38 \pm 0.04)$ eV for Ge, which agree in sign but are in order of magnitude larger than those predicted by Eq. (25). Inspite of the large experimental error, our data for silicon also indicate values of b_2 and d_2 not more than an order of magnitude larger than the predictions of the point-ion model.

Our value of $\mathcal{E}_2$ is in agreement with other measurements[4,13] and the theoretical calculation of Goroff and Kleinman.[29] The average value of $\mathcal{E}_2^*$ as determined in this experiment is in good agreement with other measurements[12] but is somewhat lower than the theoretical calculations [adjusted for $E(\Delta_2') - E(\Delta_1) = 0.8$ eV].[29,30]

In our analysis of the experimental data, we have neglected a number of possible stress-dependent effects (in addition to those mentioned in Sec. III), such as the change in exciton binding energy, stress dependence of phonon energies, and changes in the electron-phonon self-energy. Changes in the exciton binding energy can be caused by changes in the density of states as a result of the removal of degeneracies, and by the stress dependence of the v_1 band effective mass due to the v_1-v_3 coupling. Balslev[4] has shown that the density-of-states change will cause a decrease in the exciton binding energy of only about 0.5×10^{-3} eV. The v_1-v_3 coupling should also have a very small influence on the exciton binding energy since the change in the average mass of the v_1 band is zero: The stress dependence of the parallel mass is twice that of the perpendicular mass and is of opposite sign.

Recent experiments[35,36] have shown that in silicon phonon energies can change by as much as 1×10^{-3} eV at the highest stresses reached in this experiment. However, unless there is an intraband splitting of the the TO phonons involved in the indirect transitions, the stress dependence of the phonons can be assumed to be included in the Hamiltonian of Eq. (4): The interband splitting of the phonons is described by an equation of the same form as Eq. (4) except, of course, that the parameters corresponding to $\mathcal{E}_1$ and $\mathcal{E}_2$ refer to changes in phonon energies. At the present time, no information is available on the intraband splitting of the phonons.

The self-energy effect mentioned above is related to a change in band-edge energy caused by the stress dependence of the electron-(hole)-phonon interaction. The stress-induced splitting of the electronic levels will cause a change in the density of states available for phonon-assisted interband scattering. For example, such scattering will not take place when the stress-induced splitting of the electronic bands is larger than the corresponding phonon energy. Hence, if the self-energy term is significant a square root singularity should be observed at points where band splittings become equal to the corresponding phonon energy. In silicon the TO-phonon energy is 57.3×10^{-3} eV[21] and for [001] stress, the conduction-band splitting is equal to this energy at $X \approx 7\times10^{9}$ dyn cm^{-2}. Figure 4 shows no discontinuities at this stress. We have also failed to observe this effect in AlSb.[15]

A theoretical investigation of the transition intensities was also performed, which helped in analyzing the spectra of silicon near the indirect gap and yielded the first evidence of $\Delta_{5,v} \rightarrow \Delta_{1,c}$ transitions contributing to the indirect mechanisms in this material.

APPENDIX A: STRESS-DEPENDENT EIGENFUNCTIONS OF v_1, v_2 AND v_3 VALENCE-BAND LEVELS

Stress along [111]

The unperturbed wave functions for this stress direction can be written as[37]

$$\left|\tfrac{3}{2},\tfrac{3}{2}\right\rangle_{111} = \tfrac{1}{2}\left|\{(X-Y)+(i/\sqrt{3})(X+Y-2Z)\}\uparrow\right\rangle,$$

$$\left|\tfrac{3}{2},\tfrac{1}{2}\right\rangle_{111} = \tfrac{1}{6}\left|\{2\sqrt{2}\,(X+Y+Z)\uparrow + [\sqrt{3}\,(X-Y)+i(X+Y-2Z)]\downarrow\}\right\rangle,$$

$$\left|\tfrac{1}{2},\tfrac{1}{2}\right\rangle_{111} = \tfrac{1}{3}\left|\{(X+Y+Z)\uparrow - [\tfrac{3}{2}(X-Y)-(i/\sqrt{2})(X+Y-2Z)]\downarrow\}\right\rangle.$$

X, Y, and Z are the valence-band wave functions which transform as atomic p functions under the operations of the group of the tetrahedron, and $\uparrow$ and $\downarrow$ indicate spin up and spin down, respectively, referring to the stress axis. Using these functions, we calculate the following eigenfunctions of $\mathcal{H}$:

$$\left|v_2\right\rangle_{111} = \left|\tfrac{3}{2},\tfrac{3}{2}\right\rangle_{111},$$

$$\left|v_1\right\rangle_{111} = (1/q_1)[\sqrt{2}\,\delta E'_{111}\left|\tfrac{3}{2},\tfrac{1}{2}\right\rangle_{111} + (n_1-m_1)\left|\tfrac{1}{2},\tfrac{1}{2}\right\rangle_{111}],$$

$$\left|v_3\right\rangle_{111} = (1/q_1)[(m_1-n_1)\left|\tfrac{3}{2},\tfrac{1}{2}\right\rangle_{111} + \sqrt{2}\,\delta E'_{111}\left|\tfrac{1}{2},\tfrac{1}{2}\right\rangle_{111}],$$

where

$$m_1 = \bar{\Delta}_0 + \tfrac{1}{2}\delta E_{111}\,, \quad n_1 = [m_1^2 + 2(\delta E'_{111})^2]^{1/2},$$

$$q_1 = [2n_1(n_1 - m_1)]^{1/2}.$$

Stress along [001]

The unperturbed wave functions are now

$$|\tfrac{3}{2}, \tfrac{3}{2}\rangle_{001} = \sqrt{\tfrac{1}{2}}\,|(X+iY)\uparrow\rangle\,,$$

$$|\tfrac{3}{2}, \tfrac{1}{2}\rangle_{001} = \sqrt{\tfrac{1}{6}}\,|[2Z\uparrow + (X+iY)\downarrow]\rangle\,,$$

$$|\tfrac{1}{2}, \tfrac{1}{2}\rangle_{001} = \sqrt{\tfrac{1}{3}}\,|[Z\uparrow - (X+iY)\downarrow]\rangle\,.$$

The perturbed eigenfunctions in this case are similar to those defined for [111] stress, replacing δE_{111} and $\delta E'_{111}$ by δE_{001} and $\delta E'_{001}$, respectively. The quantities m_0, n_0, and q_0 are similar to m_1, n_1, and q_1 with this change.

Stress along [110]

The unperturbed wave functions have the following form:

$$|\tfrac{3}{2}, \tfrac{3}{2}\rangle_{110} = \sqrt{\tfrac{1}{2}}\,|\{Z + (i/\sqrt{2})(X-Y)\}\uparrow\rangle\,,$$

$$|\tfrac{3}{2}, -\tfrac{1}{2}\rangle_{110} = \sqrt{\tfrac{1}{6}}\,|\{\sqrt{2}\,(X+Y)\downarrow - [Z - (i/\sqrt{2})(X-Y)]\uparrow\}\rangle\,,$$

$$|\tfrac{1}{2}, -\tfrac{1}{2}\rangle_{110} = \sqrt{\tfrac{1}{3}}\,|\{\sqrt{\tfrac{1}{2}}\,(X+Y)\downarrow + [Z - (i/\sqrt{2})(X-Y)]\uparrow\}\rangle\,.$$

The perturbed eigenfunctions are computed using the procedure explained in the text, which gives

$$|v_2\rangle_{110} = \gamma_{22}|\tfrac{3}{2}, \tfrac{3}{2}\rangle_{110} + \gamma_{21}|\tfrac{3}{2}, -\tfrac{1}{2}\rangle_{110} + \gamma_{23}|\tfrac{1}{2}, -\tfrac{1}{2}\rangle_{110}\,,$$

$$|v_1\rangle_{110} = \gamma_{12}|\tfrac{3}{2}, \tfrac{3}{2}\rangle_{110} + \gamma_{11}|\tfrac{3}{2}, -\tfrac{1}{2}\rangle_{110} + \gamma_{13}|\tfrac{1}{2}, -\tfrac{1}{2}\rangle_{110}\,,$$

$$|v_1\rangle_{110} = \gamma_{32}|\tfrac{3}{2}, \tfrac{3}{2}\rangle_{110} + \gamma_{31}|\tfrac{3}{2}, -\tfrac{1}{2}\rangle_{110} + \gamma_{33}|\tfrac{1}{2}, -\tfrac{1}{2}\rangle_{110}\,.$$

The quantities γ_{ij} are given by

$$\gamma_{11} = \frac{\sqrt{2}}{q_2}\left(\delta E'_{110} - \frac{3}{32}\,\frac{1}{q_2^2}\,\frac{[\delta E'_{110}\delta\epsilon - (n_2-m_2)\,\delta\epsilon'][2\delta E'_{110}\delta\epsilon' + (n_2-m_2)\delta\epsilon]}{[2\delta E_{110} + (n_2-m_2)]n_2}\,(m_2-n_2)\right),$$

$$\gamma_{12} = -\frac{1}{q_2}\,\frac{\sqrt{6}}{8}\,[\delta E'_{110}\delta\epsilon - (n_2-m_2)\delta\epsilon']\,,$$

$$\gamma_{13} = \frac{1}{q_2}\left((n_2-m_2) - \frac{3}{16}\,\frac{1}{q_2^2}\,\frac{[\delta E'_{110}\delta\epsilon - (n_2-m_2)\delta\epsilon'][2\delta E'_{110}\delta\epsilon' + (n_2-m_2)\,\delta\epsilon]}{[2\delta E_{110} + (n_2-m_2)]n_2}\,\delta E'_{110}\right)\,,$$

$$\gamma_{21} = \frac{1}{q_2^2}\left(\frac{\sqrt{3}}{2}\right)\left(\frac{\delta E'_{110}\delta\epsilon - (n_2-m_2)\delta\epsilon'}{2\delta E_{110} + (n_2-m_2)} - \frac{2\delta E'_{110}\delta\epsilon' + (n_2-m_2)\delta\epsilon}{2[2\delta E_{110} + (n_2+m_2)]}\,(m_2-n_2)\right)\,,$$

$$\gamma_{22} = 1\,,$$

$$\gamma_{23} = -\frac{1}{q_2^2}\,\frac{\sqrt{6}}{4}\left(\frac{\delta E'_{110}\delta\epsilon - (n_2-m_2)\delta\epsilon'}{2\delta E_{110} + (n_2-m_2)}\,(m_2-n_2) + \frac{2\delta E'_{110}\delta\epsilon' + (n_2-m_2)\delta\epsilon}{2\delta E_{110} + (n_2+m_2)}\,\delta E'_{110}\right)\,,$$

$$\gamma_{31} = \frac{1}{q_2}\left((m_2-n_2) + \frac{1}{q_2^2}\,\frac{3}{16}\,\frac{\delta E'_{110}}{n_2}\,\frac{[\delta E'_{110}\delta\epsilon - (n_2-m_2)\delta\epsilon'][2\delta E'_{110}\delta\epsilon' + (n_2-m_2)\delta\epsilon]}{2\delta E_{110} - (m_2+n_2)}\right),$$

$$\gamma_{32} = \frac{1}{q_2}\,\frac{\sqrt{3}}{4}\,\frac{2\delta E'_{110}\delta\epsilon' + (n_2-m_2)\delta\epsilon}{2\delta E_{110} - (m_2+n_2)}\,,$$

$$\gamma_{33} = \frac{\sqrt{2}}{q_2}\left(\delta E'_{110} + \frac{1}{q_2^2}\,\frac{3}{32}\,\frac{(n_2-m_2)}{n_2}\,\frac{[\delta E'_{110}\delta\epsilon - (n_2-m_2)\delta\epsilon'][2\delta E'_{110}\delta\epsilon' + (n_2-m_2)\delta\epsilon]}{2\delta E_{110} - (m_2+n_2)}\right).$$

m_2, n_2, and q_2 are given by Eq. (21).

APPENDIX B: INTENSITIES OF INDIRECT TRANSITIONS

The general expression for the intensities of excitonic lines in modulated optical spectra, corresponding to TO-phonon-assisted indirect transitions between the $\Gamma_{25',v}$ valence and $\Delta_{1,c}$ conduction bands, can be written as being proportional to[38]

$$g = \left(\left|\frac{\langle\Gamma_{25',v}|\hat{e}\cdot\vec{p}|\Gamma_{15,c}\rangle\langle\Gamma_{15,c}|\mathcal{H}_p|\Delta_{1,c}\rangle}{E(\Delta_{1,c}) - E(\Gamma_{15,c})}\right|^2\right.$$

$$+\left|\frac{\langle\Gamma_{25',v}|\mathcal{H}_p|\Delta_{5,v}\rangle\langle\Delta_{5,v}|\hat{e}\cdot\vec{p}|\Delta_{1,c}\rangle}{E(\Gamma_{25',v})-E(\Delta_{5,v})}\right|^2\Bigg), \quad \text{(B1)}$$

where $\hat{e}$ is the unit polarization vector of the incident electric field, $\vec{p}$ is the linear momentum of the electron, and $\mathcal{H}_p$ is the Hamiltonian for the electron-phonon interaction. The first term on the right-hand side of Eq. (B1) represents the contribution of indirect processes using the $\Gamma_{15,c}$ conduction band as an intermediate state, while the second right-hand term is the contribution of indirect transitions via the $\Delta_{5,v}$ valence-band intermediate state.

The only nonzero matrix elements of $\hat{e}\cdot\vec{p}$ between $\Gamma_{25',v}$ and $\Gamma_{15,c}$ are given by[22,37]

$$Q=\langle X|p_y|z\rangle=\langle Z|P_y|x\rangle$$
$$=\langle Y|p_x|z\rangle=\langle Z|p_x|y\rangle$$
$$=\langle X|p_z|y\rangle=\langle Y|p_z|x\rangle\ ,$$

where x, y, and z are the basis functions of $\Gamma_{15,c}$.[37] The only nonzero matrix elements of $\hat{e}\cdot\vec{p}$ between $\Delta_{1,c}$ and $\Delta_{5,v}$ are given by[22]

$$\langle\Delta_{1,c}|p_y|\Delta_{5,v}\rangle=\langle\Delta_{1,c}|p_z|\Delta_{5,v}\rangle \quad \text{along [100]},$$

$$\langle\Delta_{1,c}|p_x|\Delta_{5,v}\rangle=\langle\Delta_{1,c}|p_z|\Delta_{5,v}\rangle \quad \text{along [010]},$$

$$\langle\Delta_{1,c}|p_x|\Delta_{5,v}\rangle=\langle\Delta_{1,c}|p_y|\Delta_{5,v}\rangle \quad \text{along [001]},$$

It has also been shown[22] that $\langle\Delta_{1,c}|\vec{p}|\Delta_{5,v}\rangle$ at the $\Delta_{1,c}$ minimum is approximately equal to $\langle\Gamma_{25',v}|\vec{p}|\Gamma_{15,c}\rangle$.

The selection rules governing the $\Gamma_{15,c}\rightarrow\Delta_{1,c}$ TO-phonon transition are given by the following expressions:[18] For a TO phonon along the [001] valleys we have

$$\langle x|\mathcal{H}_p^y|\Delta_{1,c}^{(001)}\rangle=\langle y|\mathcal{H}_p^x|\Delta_{1,c}^{(001)}\rangle\neq 0,$$

$$\langle z|\mathcal{H}_p^x|\Delta_{1,c}^{(001)}\rangle=\langle z|\mathcal{H}_p^y|\Delta_{1,c}^{(001)}\rangle=0;$$

while for a TO phonon along [010]:

$$\langle x|\mathcal{H}_p^z|\Delta_{1,c}^{(010)}\rangle=\langle z|\mathcal{H}_p^x|\Delta_{1,c}^{(010)}\rangle\neq 0,$$

$$\langle y|\mathcal{H}_p^x|\Delta_{1,c}^{(010)}\rangle=\langle y|\mathcal{H}_p^z|\Delta_{1,c}^{(010)}\rangle=0;$$

and for a TO phonon along [100]:

$$\langle y|\mathcal{H}_p^z|\Delta_{1,c}^{(100)}\rangle=\langle z|\mathcal{H}_p^y|\Delta_{1,c}^{(100)}\rangle\neq 0,$$

$$\langle x|\mathcal{H}_p^y|\Delta_{1,c}^{(100)}\rangle=\langle x|\mathcal{H}_p^z|\Delta_{1,c}^{(100)}\rangle=0.$$

For the $\Gamma_{25',v}\rightarrow\Delta_{5,v}$ TO-phonon-transition selection rules, the $\Gamma_{15,c}$ is replaced by $\Gamma_{25',v}$, and $\Delta_{1,c}$ is replaced by $\Delta_{5,v}$ in the above expressions.

We have assumed that

$$\langle\Gamma_{15,c}|\mathcal{H}_p|\Delta_{1,c}\rangle=\langle\Gamma_{25',v}|\mathcal{H}_p|\Delta_{5,v}\rangle.$$

Using the stress-dependent eigenfunctions given in Appendix A for the three stress directions, and the preceding selections rules, the theoretical peak intensities were computed for one or two intermediate states, for which case we used the approximate relation between the energy denominators[22]

$$\left(\frac{E(\Delta_{1,c})-E(\Gamma_{15,c})}{E(\Gamma_{25',v})-E(\Delta_{5,v})}\right)^{22}\approx\frac{5}{8}.$$

Table II gives these theoretical expressions obtained for the three stress directions and the different light polarizations (electric field $\vec{E}$ referred to crystal axis).

---

†Work supported by the National Science Foundation, the Advanced Research Projects Agency, and the U. S. Army Research Office (Durham).

*NASA post-doctoral International University Fellow, sponsored by the European Space Research Organization.

[1]See, for example, D. Long, J. Appl. Phys. 33, 1682 (1962).

[2]J. C. Hensel and G. Feher, Phys. Rev. 129, 1041 (1963).

[3]J. J. Hall, Phys. Rev. 128, 68 (1962).

[4]I. Balslev, Phys. Rev. 143, 636 (1966).

[5]F. H. Pollak and M. Cardona, Phys. Rev. 172, 816 (1968).

[6]G. E. Pikus and G. L. Bir, Fiz. Tverd. Tela 1, 1642 (1959)[Soviet Phys. Solid State 1, 1502 (1959)].

[7]H. Hasegawa, Phys. Rev. 129, 1029 (1963).

[8]K. Suzuki and J. C. Hensel, Bull. Am. Phys. Soc. 14, 113 (1969).

[9]S. Zwerdling, K. J. Button, B. Lax, and L. M. Roth, Phys. Rev. Letters 4, 173 (1960).

[10]H. Brooks, in *Advances in Electronics and Electron Physics*, edited by L. Marton (Academic, New York, 1955), Vol. 7, p. 85.

[11]We have used script $\mathcal{E}$'s to denote the conduction-band deformation potentials in order to avoid confusion with the symbol used for energy. A discussion of the various notations used for the deformation potentials has been given by E. O. Kane [Phys. Rev. 178, 1368 (1969)].

[12]J. C. Hensel, H. Hasegawa, and M. Nakayama, Phys. Rev. 138, A225 (1965).

[13]I. P. Akimchenko and V. A. Vdovenkov, Fiz. Tverd. Tela 11, 658 (1969)[Soviet Phys. Solid State 11, 528 (1969)].

[14]J. E. Rowe, K. L. Shaklee, and M. Cardona, Solid State Commun. 7, 441 (1969).

[15]L. D. Laude, M. Cardona, and F. H. Pollak, Phys. Rev. 1, 1436 (1970).

[16]M. Cardona, in *Modulation Spectroscopy*, edited by F. Seitz, D. Turnbull, and H. Ehrenreich (Academic, New York, 1969).

[17]Futurecraft Corp., South El Monte, Calif.

[18]E. Erlbach, Phys. Rev. 150, 2 (1967).

[19]A. Frova, P. Handler, E. A. Germano, and D. E. Aspnes, Phys. Rev. 145, 575 (1966).

[20]B. N. Brockhouse, Phys. Rev. Letters 2, 256 (1959).

[21]K. L. Shaklee and R. E. Nahory, Phys. Rev. Letters

24, 942 (1970).
[22]M. Cardona and F. H. Pollak, Phys. Rev. 142, 530 (1966).
[23]The deformation potential $\mathcal{E}_2^*$ is equal to that used in Ref. 12 (Ξ_μ').
[24]H. J. McSkimin, J. Appl. Phys. 24, 988 (1953).
[25]S. Zwerdling, K. J. Button, B. Lax, and L. M. Roth, Phys. Rev. Letters 4, 173 (1960).
[26]D. Brust and L. Liu, Solid State Commun. 4, 193 (1966).
[27]F. Cerdeira, J. S. de Witt, U. Rössler, and M. Cardona, Phys. Status Solidi 41, 735 (1970).
[28]J. C. Hensel and K. Suzuki, Bull. Am. Phys. Soc. 14, 113 (1969).
[29]I. Goroff and L. Kleinman, Phys. Rev. 132, 1080 (1963).
[30]P. J. Melz, Harvard University Technical Report No. HP-25, 1969 (unpublished).
[31]W. Paul and G. L. Pearson, Phys. Rev. 98, 1755 (1955).
[32]D. Warschauer and W. Paul, J. Phys. Chem. Solids 5, 102 (1958).
[33]M. Nathan and W. Paul, Phys. Rev. 128, 38 (1962).
[34]I. Balsley, J. Phys. Soc. Japan Suppl. 21, 101 (1966).
[35]G. S. Hobson and E. G. S. Paige, Proc. Phys. Soc. (London) 88, 437 (1966).
[36]E. Anastassakis, A. Pinczuk, E. Burstein, F. H. Pollak, and M. Cardona, Solid State Commun. 8, 133 (1970).
[37]E. O. Kane, in *Semiconductors and Semimetals*, edited by R. K. Willardson and A. C. Beer (Academic, New York, 1967), Vol. 1, p. 75.
[38]J. O. Dimmock, Ref. 37, Vol. 3, p. 296.

PHYSICAL REVIEW B VOLUME 3, NUMBER 8 15 APRIL 1971

Band-Tail Model for Optical Absorption and for the Mobility Edge in Amorphous Silicon

Frank Stern
IBM Watson Research Center, Yorktown Heights, New York 10598
(Received 18 November 1970)

The potential in amorphous Si is assumed to be the crystalline potential perturbed by a fluctuating potential with a root-mean-square amplitude $V_{\rm rms}$ and a correlation length L. The density of states for such a perturbing potential is taken from the work of Halperin and Lax. The optical absorption is calculated using effective-mass-approximation envelope wave functions whose degree of localization depends on energy. A good fit to optical-absorption data for amorphous Si films annealed at room temperature is obtained using $V_{\rm rms}=0.89$ eV and $L=6$ Å, provided the wave-vector separation between the conduction- and valence-band edges is reduced from 9.5×10^7 to 6×10^7 cm^{-1}. The mobility edge is found from an extension to the model which gives an effective bandwidth W and a spacing parameter r_s, each as a function of energy. The mobility edge E_m lies approximately where $W(E_m)=\frac{2}{3}V_{\rm rms}$. The mobility near the mobility edge is estimated from a diffusion model to be 5 cm^2/V sec, and the density of states at the edge is 10^{21} cm^{-3} eV^{-1}.

I. INTRODUCTION

A substantial body of information has accumulated concerning the properties of amorphous semiconductors, particularly in the last two years.[1] Many models for describing the properties of these materials have evolved,[2,3] and some features of these models are reflected in the work reported in this paper. We calculate the electrical and optical properties of amorphous Si from a model which assumes that the amorphous material is a strongly perturbed crystal. That is, we start with the energy gap, dielectric constant, and effective masses of the crystal, introduce a strong randomly varying perturbing potential of a particular form, and ask for the resulting density of states, wave functions, optical absorption, and dc conductivity.

In the course of the calculation we make many assumptions and approximations. Some of these are justified by qualitative reasoning, guided by knowledge of the behavior at high or low energies. Others are made simply to permit numerical results to be obtained without excessive computation. We believe that the resulting model has the advantage of allowing the microscopic properties of the system to be exhibited quantitatively.

The model is applied to amorphous Si, whose optical and electrical properties have been investigated by many authors, and for which the relevant parameters of the crystal are well known. The method is applicable to other amorphous semiconductors, such as the chalcogenides and their alloys, provided band-structure parameters and dielectric constants are known.

II. DENSITY OF STATES

The first quantity we need to know is the density of states in each band. Throughout the calculation we adopt the sign convention that energies in the tail are negative and energies well into the band are positive, and use the nominal (i.e., unperturbed) band edge as the zero of energy for each